CHIN. PHYS. LETT. Vol. 30, No. 7 (2013) 076202

The Material Behavior and Fracture Mechanism of a Frangible Bullet Composite *

LI Jian(李健)[1], RONG Ji-Li(荣吉利)[2**], ZHANG Yu-Ning(张豫宁)[1], XU Tian-Fu(徐天富)[2], LI Bin(李彬)[1]

[1]*Guangxi Key Laboratory of Automobile Components and Vehicle Technology, Guangxi University of Science and Technology, Liuzhou 545006*

[2]*School of Aerospace Engineering, Beijing Institute of Technology, Beijing 100081*

(Received 28 April 2013)

The quasi-static and dynamic compressive mechanical properties of a bullet composite are investigated using the scattered spot technique, an electronic universal testing machine, and a Split–Hopkinson pressure bar. The stress-strain curves under static and dynamic loading are also obtained, and the strain rate effect is analyzed. The rupture structure is observed under a scanning electron microscope, and the microscopic damage mechanism of the bullet composite is examined. Results show that the composite is sensitive to the strain rate, such that the compressive strength of the composite increases with increased strain rate. The relationship of the compressive strength and elastic modulus with the logarithmic strain rate is nonlinear.

PACS: 62.20.mm 81.05.Lg DOI: 10.1088/0256-307X/30/7/076202

Frangible bullets are a type of ammunition that combine new principles with a new material, and are thus a current research hotspot. Most of the frangible bullets studied are enclosed in a shell and mainly used for tank armor or reinforced concrete. In general, frangible bullets are made of depleted uranium, pure tungsten, or high-proportion tungsten alloy.[1−3] Teyfik *et al.*[4] experimentally investigated the impact behavior of aluminum alloys 7075 and 5083 and the high-strength low-alloy steel AISI 4140 under a 7.62 mm armor-piercing projectile. Sukumar *et al.*[5] studied the ballistic impact behavior of the high-strength near-beta Ti alloy β-CEZ under different micro-structural conditions against 7.62 mm armor-piercing projectiles. Wu *et al.*[6] investigated the microstructure and mechanical properties of a new type of tungsten alloy used in a penetrator by powder metallurgy methods, whereas Du *et al.*[7] used four different tungsten alloy materials to establish the relationship between the dynamic penetration performance of the frangible material and the static testing parameters. In addition, Hazell *et al.*[8] examined the fracture surfaces and failed cross-sections under light optical and scanning electron microscopy, and related the findings to the microstructure of the composite bullet.

Many researchers have studied composite bullets in recent years. Banovic[9] observed the microscopic fracture mechanisms of Cu-Sn frangible bullets under quasi-static and dynamic compression, and Pradipta *et al.*[10] studied the material behavior against 7.62 mm deformable projectiles and explored the behavior of a high-strength armor steel in two different tempering conditions against 7.62 mm deformable projectiles. Mates *et al.*[11] examined the fracture surfaces and failed cross sections of a composite bullet microstructure via scanning electron microscopy.

Thus, traditional frangible bullets are mostly manufactured with tungsten alloy material. On the one hand, the merits of these bullets are high kinetic energy and strong penetrating power, and they are mainly used for tank armor or reinforced concrete. On the other hand, the defect is a complicated process, with high cost and the inability to satisfy application requirements in special situations. While the characteristics of composite frangible bullets are low cost, penetrability to some extent, and they are frangible and do not excessively rebound and run through targets, so they do not endanger non-targets and innocent people.

In this Letter, we propose a material for frangible bullets that is not a tungsten alloy, but a composite containing mixed and sintered metals and organics. These materials have penetrability to some extent, but are more frangible than the tungsten alloy. These frangible bullets are a new type of ammunition that possess frangibility, weak penetrating power, and are low cost. This kind of frangible bullet can be used by the police, army and aircraft police when carrying out missions. Research on frangible bullet composites is limited, and practical applications require further studies. Thus, the development of a frangible, weakly penetrating, low-cost bullet has practical significance.

The mechanical properties of the proposed material for frangible bullets are examined under quasi-static and dynamic loading. The properties include tensile strength, compressive strength, and stress-strain relationship. The dynamic behavior of the frangible bullet composite is determined by a Split–Hopkinson pressure bar (SHPB) experiment based on a quasi-static test. Scanning electron microscopy (SEM) analysis is also performed to investigate the microscopic and macroscopic structural changes of the frangible bullet's compressive fracture. The organizational structure of the material after compressive failure is observed, the failure mechanisms of the compos-

*Supported by the National Natural Science Foundation of China under Grant Nos 10972033 and 51209042.

**Corresponding author. Email: rongjili@bit.edu.cn

© 2013 Chinese Physical Society and IOP Publishing Ltd

ite are analyzed, and stress-strain curves under quasi-static and impact loading are constructed.

Small-caliber frangible bullets that possess frangibility, weak penetrating power, and are low cost have extensive application prospects in the international market. Research on small-caliber frangible bullets can promote the development and commercial value of domestic ammunition technology.

The proposed frangible bullet material is a kind of composite containing mixed and sintered metals and organics. Thus, the composition and mechanical properties of the material are experimentally examined by initially determining the relative elemental contents of the composite. Subsequently, the bullets are processed to become experimental samples, whose properties under quasi-static and dynamic loading are then analyzed.

Micro-spectrum analysis technology and chemical analysis are performed to determine the relative elemental contents of the composite, and the results are shown in Table 1. Unlike conventional bullets, the composite-made frangible bullets are not entirely made of metal, and are comprised of about 30% nonmetallic elements.

The quasi-static mechanical properties of the material are examined by processing the bullets into long cylindrical and flat cylindrical specimens. A tensile machine combined with the pasting strain-gauge method and the three-dimensional scattered-spot method is used to investigate the compressive and tensile properties of the material. Given that frangible bullets are kinetic-energy bullets, the properties of the composite under impact loading must be examined to develop and optimize the frangible bullet composite. The strain-rate and stress-strain properties of the composite under impact loading are also studied using an SHPB.

A tensile machine combined with the pasting strain-gauge method is used to study the elastic modulus, Poisson ratio, and compressive strength of the material. The beam of the tensile machine constantly moves down and directly acts on the specimen. The mechanical parameters of the material are measured using pasting strain gauges along the axle and radius directions of the specimen. The elastic modulus, yield stress, and compressive strength limitation are determined by the force-displacement curve, and the Poisson ratio is determined using the strain-gauge data.

The tensile properties of the material are examined by a quasi-static compressive test using an electronic universal testing machine and the three-dimensional scattered-spot method. Force is applied onto the flat cylindrical specimen along the diameter direction, and the two parts perpendicular to the applied-force direction are affected by tension. When the stress value exceeds the tensile strength of the material, tensile fracturing occurs in the specimens. Black and white paint are first alternately sprayed on the surface of the specimen, which forms an artificial speckle pattern. The specimen is then placed in the electronic universal testing machine for compressive loading. The surface of the specimen is irradiated with cold light. Meanwhile, the speckle images of the specimen surface are recorded during the deformation process using two CCD cameras. The initial time and deformation results are shown in Fig. 1. Finally, the stress-strain curves and tensile strength of the material can be calculated using analysis software.

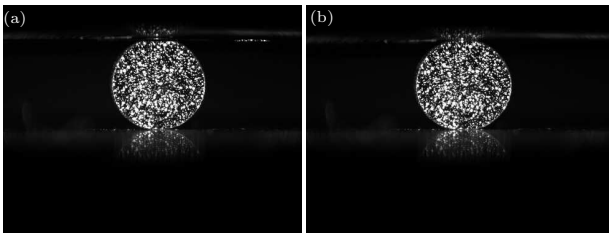


Fig. 1. Speckle images of the surface of the specimen in a quasi-static compressive test: (a) initial time, (b) structural deformation.

The SHPB is widely used to investigate the compressive, tensile, and fracture properties of composites under different impact loadings and varied strain rates. The high-strain-rate properties of composites have been extensively studied in the past decade.[12] Manmohan *et al.*[13] investigated the compression behavior of aluminum syntactic foam and established full stress-strain diagrams for strain rates ranging from quasi-static to $1400\,\mathrm{s}^{-1}$ using a modified SHPB. They found that the foam appears to be more sensitive to the strain rate. We previously investigated the dynamic fracture properties and damage mechanism of glass fiber polymer composite-embedded ZnO whiskers by using a Split–Hopkinson pressure bar,[14] and found that the mass percentage of ZnO has little influence on the dynamic fracture toughness. Xue *et al.*[15] investigated the behavior of porous iron under compression loading using a servo-hydraulic machine and an SHPB. They found that the material has bilinear behavior over the tested strain rates. The porosity directly affects the yield strength and post-yield behavior of the material. We also previously investigated the dynamic tensile properties of glass-fiber polymer composites embedded with ZnO whiskers by SHPB and discussed the strain rate effect on the mechanical behavior.[16]

The failure characteristics of the composite in the test have been extensively elucidated by analyzing the composite's fracture surface in past research. Liu *et al.*[17] evaluated the microstructure, micro-hardness dry sliding and wear resistance of Cr3Si/γ-Fe composite coating by SEM. Yue *et al.*[18] studied the excellent sensing properties of the $ZnOSnO_2$ composite via SEM and transmission electron microscopy, and Lan *et al.*[19] observed the surface morphologies of TiO_2 films by SEM. They found that the surface morphologies of TiO_2 films are determined not only by the dispersion methods, but also by the percentage of TiO_2

powder in the dispersing system. CAO *et al.*[20] studied the dynamic response and fracture mechanism of novel structural radar absorbing material by means of the split Hopkinson pressure bar (SHPB) and SEM.

To explain the failure characteristics of the composite in the test intuitively and to understand the anti-impact performances of different components of the composite, the rupture sections of the specimens are observed by the SEM method. The relationship between the structure and properties of the composite is determined, and the failure mechanisms of the composite are analyzed.

Table 1. The relative elemental contents of the composite.

Elements	S	K	Ca	Fe	Cu	W
Relative contents (%)	21.29	6.38	1.13	1.20	30.49	39.51

Table 2. The geometric dimensions of the specimens in the test.

Serial number	Dimensions of specimens		Experiment items
	Diameter (mm)	Length (mm)	
1	6	14	Compressive strength
2	9	4	Tensile strength
3	10	12	Dynamic compressive strength

Table 3. The parameters of the material under quasi-static loading.

Property	9.37 (10^{-4}s^{-1})	1.35 (10^{-3}s^{-1})	1.62 (10^{-4}s^{-1})
Compressive strength (MPa)	29.7	30	31.2
Tensile strength (MPa)	4.6	4.3	4.5
Elastic modulus (MPa)	1176	1198	1270
Poisson ratio	0.319	0.327	0.317

Table 4. The parameters of the specimens under dynamic loading.

Property	1030 s^{-1}	1580 s^{-1}	1628 s^{-1}	1750 s^{-1}	1900 s^{-1}
Compressive strength (MPa)	95	100	101	103	104
Failure strain	0.0062	0.0083	0.0051	0.0054	0.0045
Elastic modulus (GPa)	18.43	19.62	20.75	22.43	23.87

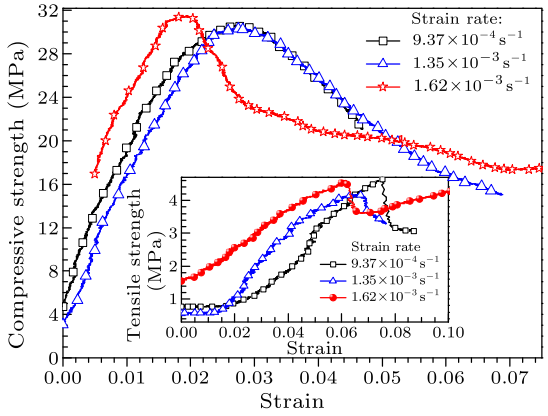


Fig. 2. The stress-strain curves of the specimen under quasi-static loading.

The geometric dimensions of the specimens used in the aforementioned test are listed in Table 2. Figure 2 shows the compressive strength-strain curve of specimens under quasi-static loading. The inset is the tensile strength-strain curve of the specimens, and the curves are obviously nonlinear. The yield stage of the material is not obvious. The compressive strength is not high, i.e., between 29 and 32 MPa, and the tensile strength is very low, i.e., between 4.3 and 4.6 MPa.

Quasi-static compression tests of the composite are conducted a total of six times. The test for measuring the compressive strength of the long cylindrical specimen and measuring the tensile strength of the flat cylindrical specimens are conducted three times. By controlling the downward speed of the tensile machine's beam to change the strain rates of the specimen in the compressive process, the strain rates are fixed between 9.37×10^{-4} s^{-1} and 1.62×10^{-3} s^{-1}. The load values, specimen deformation values, and strain values of each sampling point in the experiment can be obtained and used to determine the quasi-static mechanics parameters of the composite, and the results are listed in Table 3.

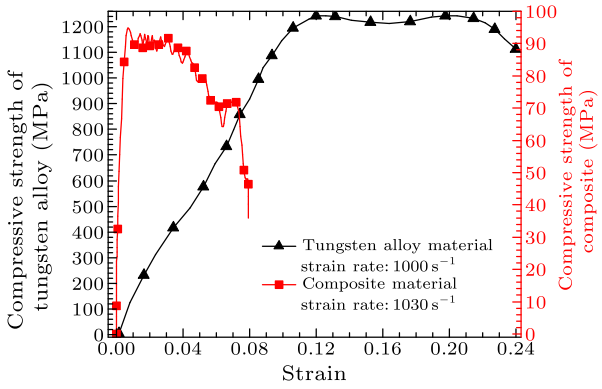


Fig. 3. The compressive strength-strain curves of two materials.

The failure modes of the frangible bullet composite under quasi-static loading are shear fracture and stratified damage. Banovic *et al.*[21] also found a similar failure mode in a study on the compressive properties and failure mechanisms of Cu-Sn frangible bullets. The damage angle and corresponding fracture strengths of the material increases with increasing strain rate.

To verify that the composite studied is suitable to be a frangible bullet core material, we compare the dynamic compressive strength of the composite under a strain rate of 1030 s^{-1} with the dynamic compressive strength of the tungsten alloy material, which was tested by Dong *et al.*[22] under a strain rate of

$1000\,\mathrm{s}^{-1}$; the curves are shown in Fig. 3. It is illustrated that the dynamic compressive strength of the composite is 95 MPa, while that of the tungsten alloy material is 1240 MPa, and this value is 13 times that of the composite. This means that the composite is more frangible than the tungsten alloy material.

Figure 4 shows the dynamic compressive stress-strain curves of the composite. The curves are linear in the initial loading stage, and they belong to elastic deformation. The curves obviously present nonlinear characteristics and the material has an apparent yield stage with increased load. When the stress reaches the limitation, the specimens undergo compressive failure. The curves decline when the strain value is >0.01, i.e., the material has no load-bearing capacity. The ultimate strength of the specimens is not high within 1000–$2000\,\mathrm{s}^{-1}$, i.e., about 103 MPa.

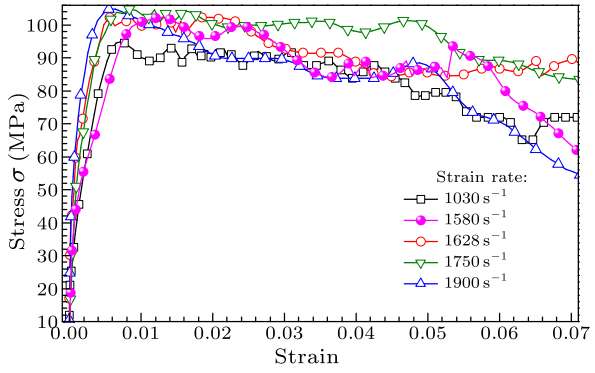


Fig. 4. The dynamic compressive stress-strain curves of the specimens.

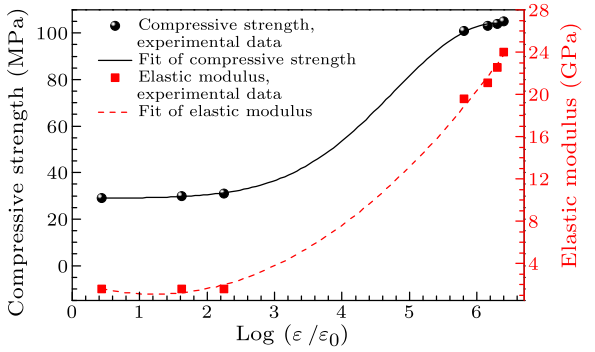


Fig. 5. The compressive strength and elastic modulus of the composite under different strain rates.

The SHPB experiments are conducted a total of five times by controlling the speed of the projectiles in the SHPB system to change the strain rate of the specimen in the compressive process. The strain rates are between $1000\,\mathrm{s}^{-1}$ and $2000\,\mathrm{s}^{-1}$. The strain values, stress values, and elastic-wave velocity values of each sampling point in the experiment can be obtained and used to determine the dynamic mechanics parameters of the composite. The results are shown in Table 4.

The correlation of the elastic modulus and compressive strength with the strain rate by the constructing curves of the compressive strength and elastic modulus vs the logarithmic strain rate is shown in Fig. 5. The composite has a strain-rate reinforcement effect, i.e., both the compressive strength and elastic modulus increase with the increasing strain rate. The relationship of the compressive strength and elastic modulus with the logarithmic strain rate is nonlinear, i.e., the composite has a nonlinear strain-rate strengthening effect.

Figure 5 also shows that the quasi-static compressive strength is about 30 MPa. By contrast, the dynamic compressive strength reaches 105 MPa when the strain rate is $1900\,\mathrm{s}^{-1}$, and this value is 3.5 times that of the quasi-static's compressive strength. Thus, the composite shows strain-rate sensitivity in the compressive process. In this study, the strain-rate sensitive coefficient proposed by Suo *et al.*[23] is used to discuss the strain-rate sensitivity of the composite. By defining the strain-rate-sensitive coefficient as m, the formula is as follows:

$$m = \frac{\partial \ln \sigma}{\partial \ln \varepsilon} = \frac{\log(\sigma_2/\sigma_1)}{\log(\dot{\varepsilon}_2/\dot{\varepsilon}_1)}, \tag{1}$$

where $\dot{\varepsilon}_1$ is the reference strain rate, σ_1 is the failure stress under a reference strain rate, $\dot{\varepsilon}_2$ is the true strain rate, and σ_2 is the failure stress under the true strain rate. The value of m indicates the incremental stress with the increasing unit strain rate and depends on the material, the size of the crystal, the dislocation density, the deformation temperature, and the strain rate. When $m > 0$, the flow stress of the material improves with the increasing strain rate. When $m < 0$, the flow stress decreases with the increasing strain rate. When $0.3 < m < 1$, the material has super-plasticity.[24–26]

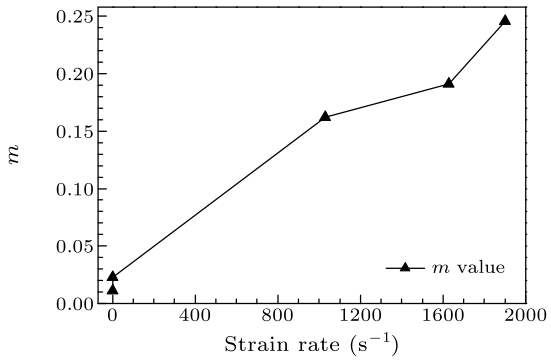


Fig. 6. The curves of the strain-rate-sensitive coefficient vs the strain rate.

By considering the ultimate strengths of the quasi-static and dynamic conditions, the strain-rate-sensitive coefficients of the quasi-static and dynamic conditions can be calculated. The calculated strain rates are from $9.37 \times 10^{-4}\,\mathrm{s}^{-1}$ to $1.62 \times 10^{-3}\,\mathrm{s}^{-1}$ under the quasi-static, and from $1000\,\mathrm{s}^{-1}$ to $1900\,\mathrm{s}^{-1}$ under the dynamic condition. The results are shown in Fig. 6. The material is insensitive to the strain rate in the area of low strain rate, and the sensitivity coefficient is very low. On the other hand, the material is

sensitive to the strain rate in the area of high strain rate, and the sensitivity coefficient is higher than that for the low strain rate. Thus, the strain rate sensitivity of the composite increases from quasi-static to dynamic conditions. The experimental results show that m increases with the increasing strain rate and that the increasing strain rate can lead to increasing stress.

To elucidate the failure characteristics of the composite in the test, SEM is performed to analyze the rupture surface of the specimens. The relationship of the material's transformation from microscopic deformation to macroscopic deformation, as well as the failure characteristics and failure mechanisms of the composite in the test, are also determined.

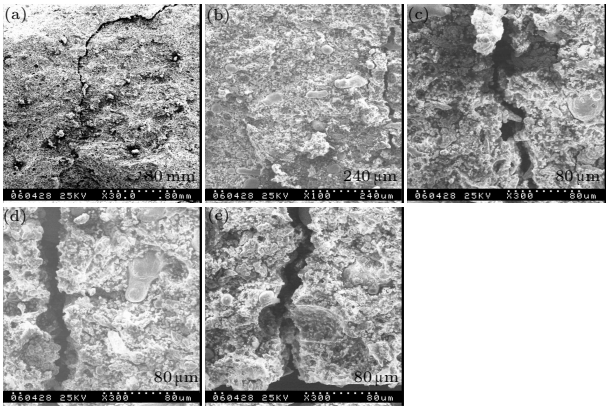


Fig. 7. The microscopic appearance of the composite after fracturing for different strain rates: (a) $1030\,\mathrm{s}^{-1}$, (b) $1580\,\mathrm{s}^{-1}$, (c) $1628\,\mathrm{s}^{-1}$, (d) $1750\,\mathrm{s}^{-1}$, (e) $1900\,\mathrm{s}^{-1}$.

Figure 7 shows SEM images of polished, washed, soaked in liquid acetone, and cleaned bullet composite. The metal material is the larger bulk surrounded by organic material (small particles). Figure 7(a) shows that the edge of the specimen is approximately 25° of the fracture angle. Both metal and organic materials exist around the crack, and organic materials are dominant and have a higher residual stress-strain concentration at a high strain rate. The metal materials are influenced by shear stress and squeezed by organic materials on both sides. With the increasing strain rate, the metals and organic particles are compressively deformed along the loading direction to adapt to the strain needs. Taking into account the change in cracks in Figs. 7(a)–7(e), the cracks and damage are deduced to be further aggravated with the increasing strain rate. They begin to be destroyed at the boundary position and then slip to produce the entire fracture surface. Ultimately, tiny macroscopic cracks develop, and the main compressive failure mode of the composite at high strain rates is therefore the shear fracture of metals and organic particles along the loading direction. With the increasing strain rate, the angles and sizes of the cracks constantly increase, and the compressive strength of the composite also continuously increases. The experimental results are the same as those of Narayanan and Linda.[27]

In summary, quasi-static and dynamic compressive loading experiments are carried out to measure the compressive strength, tensile strength, failure strain, and elastic modulus magnitudes of a frangible bullet composite. Stress-strain curves are then constructed. The composite is found to have a nonlinear strain-rate reinforcement effect, i.e., both the compressive strength and elastic modulus increase with the increasing strain rate. The composite is also found to be strain-rate sensitive, and the strain-rate sensitive coefficient is used to determine the material's strain-rate sensitivity. With the increasing strain rate, m increases, which shows that the increasing strain rate can lead to increased stress. Finally, the observed failure modes and failure mechanisms of the composite are observed with a high-speed camera, and macroscopic and microscopic images are obtained.

References

[1] Zhang C X, Qin L B and Mi W Y 2006 *Powder. Met. Mater. Sci. Eng.* **11** 127
[2] Zhang C X, Fan A G and Tian H 2003 *Ordnance Mater. Sci. Eng.* **26** 63 (in Chinese)
[3] Pradipta K, Bidyapati M, Siva K and Balakrishna T 2010 *Mater. Des.* **31** 3308
[4] Teyfik D, Mustafa Ü and Orhan R Y 2008 *Mater. Des.* **29** 2009
[5] Sukumar G, Bhav S and Bhattacharjee A 2013 *Int. J. Impact Eng.* **54** 149
[6] Wu X F, Cheng X W and Cai H N 2007 *Ordnance Mater. Sci. Eng.* **30** 46 (in Chinese)
[7] Du Z H, Shen P H and Zhao G Z 2006 *J. Ballist.* **18** 51
[8] Hazell P J, Appleby G J and Philbey D 2013 *Int. J. Impact Eng.* **54** 11
[9] Banovic S W 2007 *Mater. Sci. Eng.* A **460** 428
[10] Pradipta K J, Bidyapati M and Siva K 2010 *Mater. Des.* **31** 3308
[11] Mates S P, Rhorer R and Banovic S 2008 *Int. J. Impact Eng.* **35** 511
[12] Rong J L, Wang D, Wang X et al 2013 *Chin. Phys. Lett.* **30** 016203
[13] Manmohan D G, Marco P and George S 2012 *Mater. Des.* **42** 418
[14] Rong J L, Wang X and Cao M S 2010 *Chin. Phys. Lett.* **27** 086201
[15] Xue P, Naveed I, Liao H J et al 2012 *Int. J. Impact Eng.* **48** 82
[16] Rong J L, Wang X, Cao M S et al 2010 *Chin. Phys. Lett.* **27** 066201
[17] Liu Y F, Chen D Q and Han J M 2009 *Chin. Phys. Lett.* **26** 095202
[18] Yue X J, Hong T S, Xiang W et al 2012 *Chin. Phys. Lett.* **29** 120702
[19] Lan X H, Yang S Q, Zou Y et al 2007 *Chin. Phys. Lett.* **24** 3567
[20] Cao M S, Zhou W, Qu G M et al 2008 *Chin. Phys. Lett.* **25** 2954
[21] Banovic S W and Mates S P 2008 *J. Mater. Sci.* **43** 4840
[22] Dong K K, Sunghak L and Heung S S 1998 *Met. Mater.* **4** 508
[23] Suo T, Chen Y Z and Li Y L 2013 *Mater. Sci. Eng.* A **560** 545
[24] Akhtar S K and Liu H W 2012 *Int. J. Plast.* **36** 1
[25] Luo J and Li M Q 2012 *Mater. Sci. Eng.* A **538** 156
[26] Zhao Y P and Liu S 2001 *Chin. J. Aeronaut.* **14** 78
[27] Narayanan S and Linda S S 1999 *Compos. Sci. Technol.* **56** 1589